AAS 14-224

# LONG-TERM ORBITAL PROPAGATION THROUGH DIFFERENTIAL ALGEBRA TRANSFER MAPS AND AVERAGING SEMI-ANALYTICAL APPROACHES

**Alexander Wittig[*], Roberto Armellin[†], Camilla Colombo[‡], Pierluigi Di Lizia[§]**

Orbit perturbations are fundamental when analyzing the long-term evolution and stability of natural or artificial satellites. We propose the computation of transfer maps for repetitive dynamical systems as a novel approach to study the long-term evolution of satellite and space debris motion. We provide two examples of this technique, the evolution of high area-to-mass ratio spacecraft under solar radiation pressure and $J_2$, and a sun-synchronous groundtrack repeating orbit with drag and $J_2$. The results presented demonstrate the potentiality of the transfer maps for these problems. We furthermore compare this approach with averaging methods for the propagation of the orbital dynamics on the long-term, and suggest possibilities to combine differential algebra based methods with orbital elements averaging.

## INTRODUCTION

The effect of orbit perturbations is fundamental when analyzing the long-term evolution and stability of the motion of natural or artificial satellites in a planet-centered dynamics. Solar radiation pressure and planetary oblateness are essential to predict the motion of impact ejecta from Phobos and Deimos on orbits around Mars or high area-to-mass spacecraft around the Earth.[1,2] Similarly, space debris evolution environment models implement the effect of atmospheric drag, solar radiation pressure, anomaly of the Earth's gravity field and luni-solar perturbations.[3]

An elegant and efficient approach to analyze the effect of orbit perturbations is the semi-analytical technique based on averaging, which separates the constant, short periodic and long-periodic terms of the disturbing function. When the separation cannot be readily accomplished, the averaging technique can be used to eliminate the short-term effect of perturbations, by averaging the variational equations (or the corresponding potential) over one orbit revolution of the small body, and sometimes doubly averaging on the orbital period of an external perturbing body. Averaging corresponds to filtering the higher frequencies of the motion (periodic over one orbit revolution), which normally have small amplitudes. This allows a deeper understanding of the dynamics, to identify equilibrium solutions, librational or rotational solutions. The disturbing potential, written in Keplerian elements,

[*] AstroNet II Experienced Researcher and Postdoctoral Fellow, Department of Aerospace Science and Technology, Politecnico di Milano, 20156 Milan, Italy, alexander.wittig@polimi.it

[†] Lecturer in Astronautics, School of Engineering Sciences, University of Southampton, Southampton, SO17 1BJ, UK, roberto.armellin@soton.ac.uk

[‡] Marie Curie Research Fellow, Department of Aerospace Science and Technology, Politecnico di Milano, 20156 Milan, Italy, camilla.colombo@polimi.it

[§] Postdoctoral Fellow, Department of Aerospace Science and Technology, Politecnico di Milano, 20156 Milan, Italy, pierluigi.dilizia@polimi.it

or a set of non-singular elements, or canonical elements such as the Delaunay variables, is averaged over the fast variable, such as the true anomaly or the mean anomaly; then, the Lagrange's planetary equations are numerically integrated to obtain an accurate estimation for the secular and long term time history.

The computation of transfer maps for repetitive dynamical systems is proposed as a novel approach to study the long-term evolution of satellites motion around the Earth. The method has long been used in the area of accelerator physics to quickly and accurately study long-term evolution of particles in accelerators and storage rings.[4,5] In particular, differential algebra techniques are applied to compute a polynomial expansion of a transfer map linking the initial conditions $\boldsymbol{X}_i$ to the resulting final conditions $\boldsymbol{X}_f = P(\boldsymbol{X}_i)$ after one revolution around the Earth, about some reference orbit.[6] Once this relationship is known, propagation of a point or set of points can be performed by a simple evaluation of the polynomial $P$ which is much faster than an integration of the full equations of motion for one turn. Long-term propagation of a given initial condition can be performed by repetitive tracking, i.e., the repeated evaluation of the polynomial map $P$, provided the final condition $\boldsymbol{X}_f$ after each turn stays close to the reference orbit around which the expansion is computed. This restriction is required to ensure that the result of the previous evaluation of $P$ remains within the radius of convergence of $P$, which can be suitably tuned by varying the order of the polynomial expansion.

Fortunately, in the unperturbed two-body problem all orbits are fixed points of the transfer map, i.e., the transfer map is the identity. Introducing small perturbations, this property will of course be lost, but the overall behavior is not expected to change drastically so that the condition for repetitive tracking is satisfied. However, e.g., with third-body perturbations, the equations of motion become heavily time dependent. This means that a single map $P$ cannot express the dependence of final conditions on initial conditions accurately for all times any more. Instead, also the map $P$ must be replaced by a sequence of maps $P_t$, each expanded with respect to time as well as the initial conditions and valid only in a certain time interval. If the time dependence of the perturbing force is slow compared to the time required for one revolution of the object around the Earth, a single map $P_t$ can be valid for many revolutions before becoming inaccurate.

Within this approach, the equations of motion are written in orbital parameters and the time $t$ is replaced as the independent variable by the true anomaly $\nu$. As in averaging techniques, this allows to easily compute a one turn map by integrating from $0$ to $2\pi$. It furthermore allows the straightforward expansion of the map $P$ with respect to time without introducing further variables.

This article proposes a comparison between semi-analytical techniques and Differential Algebra techniques for the long term propagation of spacecraft and space debris objects. In particular, we introduce two Differential Algebra based methods, the well known DA integration method and the novel DA map transfer method. The orbit perturbations implemented in the dynamics are solar radiation pressure, corrections to Earth's gravitational field due to $J_2$, and atmospheric drag.

Various examples comparing direct integration of the equations of motion with the proposed map-based approach, as well as with an averaging semi-analytical technique developed for the propagation of spacecraft in the Earth's environment are presented.[7] Comparisons are made on accuracy and computational time. Moreover, the underlying relation between transfer maps approach and averaging techniques is discussed and analyzed. Indeed, these insights allow the possible integration of the differential algebra approach with averaging techniques.

As test cases we analyze the evolution of high area-to-mass ratio spacecraft under the effect of

solar radiation pressure and $J_2$ and the evolution of LEO spacecraft, under the effect of aerodynamic drag and Earth's oblateness. The results presented demonstrate the potentiality of the transfer map approach to the study of the long-term stability of planetary-centered orbits. Furthermore, it is highlighted that it may be possible to combine this approach with averaging semi-analytical methods to further extend the time validity of the transfer map.

In the following section, we introduce the dynamics considered in this paper along with a brief introduction of the semi-analytical averaging of these equations. Proceeding from there, in the next section we introduce differential algebra techniques, which can be thought of as a logical continuation of these methods. As part of this, we will briefly introduce an important DA method for the expansion of the flow of an ODE. This is followed by a detailed theoretical introduction of the DA mapping propagation technique, with applications to two test cases following. We close by summarizing our results and providing an outlook for further research.

## SEMI-ANALYTICAL APPROACH FOR ORBITAL DYNAMICS

The orbit evolution in the Earth environment can be expressed in terms of variation of orbital parameters through variational equations in Gauss' form or Lagrange's form.[8]

When the long-term propagation of the dynamics is requited, it is convenient to separate the disturbing function (or disturbing force) in terms of its constant component, short period variations and long period variations. In particular, it is possible to isolate the secular and the long-period effects on the dynamics by eliminating the short period term through the averaging technique. The most common form is obtained by averaging the perturbation over one orbit revolution. Considering that the evolution of the semi-major axis $a$, eccentricity $e$, inclination $i$, anomaly of the ascending node $\Omega$ and anomaly of the pericenter $\omega$ are much slower than the true anomaly $\nu$ or mean anomaly $M$, the variational equations can be integrated on $\nu$ or $M$ from 0 to $2\pi$, considering the other orbital elements constant over one revolution. The averaged dynamics can then be numerically integrated to account for the variation of the orbital elements over the long period. The osculating terms can also be retried a posteriori.

In this article we consider the effects of some of the main perturbations for Earth-centered orbits including aerodynamic drag, solar radiation pressure and the effect of the Earth's oblateness. The acceleration due to atmospheric drag is expressed as:

$$\mathbf{a}_{DRAG} = -\frac{1}{2} c_D \frac{A}{m} \rho v^2 \mathbf{v}$$

where $v$ is the spacecraft velocity relative to the atmosphere, $\rho$ the atmosphere density, $c_D$ the drag coefficient and $A/m$ the area-to-mass ratio of the spacecraft with $A$ the cross section area perpendicular to the velocity vector. In this article we consider a time-independent, spherically-symmetric atmosphere with a density that varies exponentially with altitude $h$, according to

$$\rho = \rho_0 \exp\left[-\frac{h - h_0}{H}\right]$$

where $\rho_0$ is the reference density at the reference altitude $h_0$ and $H$ is the scale height, whose values are taken from the literature.[9] The satellite is also subjected to the acceleration due to solar radiation pressure given by

$$\mathbf{a}_{SRP} = a_{SRP} \boldsymbol{n} \tag{1}$$

where $\mathbf{n}$ is the unit vector directed from the Sun to the center of the Earth and $a_{SRP}$ is the characteristic acceleration:

$$a_{SRP} = \frac{p_{SR} c_R A}{m} \tag{2}$$

with $p_{SR}$ the is the solar pressure $p_{SR} = 4.56 \cdot 10^{-6} N/m^2$, $c_R$ the reflectivity coefficient, and $A/m$ the area-to-mass ratio of the spacecraft with $A$ the cross section area exposed to the Sun. The effect of eclipses is neglected for the moment. Finally, the acceleration due to the Earth's oblateness coefficient $J_2$ in cartesian coordinates can be expressed as:

$$\boldsymbol{a}_{J_2} = -\frac{J_2 \mu R_E^2}{r^5} \begin{pmatrix} x\left(1 - \frac{5z^2}{r^2}\right) \\ y\left(1 - \frac{5z^2}{r^2}\right) \\ y\left(3 - \frac{5z^2}{r^2}\right) \end{pmatrix}. \tag{3}$$

Equations 1, 2, and also 3 after projecting the accelerations in the radial, transverse and normal directions, can be inserted into the Gauss's form of planetary equations to be numerically integrated.[8] When altitude is above $1000$ km, the effect of aerodynamics drag can be neglected. The secular and long-period rate of change of the orbital elements due to SRP and $J_2$ is given for example by Krivov et al.[1] and were implemented in the PlanODyn suite[7] as:

$$\begin{aligned} \frac{d\overline{\Omega}}{dt}_{J_2} &= -\frac{3}{2} J_2 \left(\frac{R_E}{a}\right)^2 \frac{n}{(1-e^2)^2} \cos i \\ \frac{d\overline{\omega}}{dt}_{J_2} &= \frac{3}{4} J_2 \left(\frac{R_E}{a}\right)^2 \frac{n}{(1-e^2)^2} \left(5\cos^2 i - 1\right) \end{aligned} \tag{4}$$

for the Earth oblateness, where $J_2 = 1.083 \cdot 10^{-3}$, $R_E$ is the radius of the Earth and $n$ the orbital mean motion, and

$$\begin{aligned} \frac{d\overline{e}}{dt}_{SRP} &= \frac{3}{2} \frac{n a_{SRP} a^2}{\mu} \sqrt{1-e^2} \sum_{k=1}^{6} A_k \sin \alpha_k \\ \frac{d\overline{i}}{dt}_{SRP} &= \frac{3}{2} \frac{n a_{SRP} a^2 e}{\mu \sqrt{1-e^2}} \cos \omega \sum_{k=7}^{9} A_k \sin \alpha_k \\ \frac{d\overline{\Omega}}{dt}_{SRP} &= \frac{3}{2} \frac{n a_{SRP} a^2 e}{\mu \sin i \sqrt{1-e^2}} \sin \omega \sum_{k=1}^{6} A_k \sin \alpha_k \\ \frac{d\overline{\omega}}{dt}_{SRP} &= -\cos i \frac{d\overline{\Omega}}{dt}_{SRP} + \frac{3}{2} \frac{n a_{SRP} a^2}{\mu} \frac{\sqrt{1-e^2}}{e} \sum_{k=1}^{6} A_k \sin \alpha_k \end{aligned} \tag{5}$$

The coefficients $A_1$ to $A_9$ and the angles $\alpha_1$ to $\alpha_9$ are function of the orbit orientation $i$, $\Omega$, $\omega$, and the longitude of the Sun on the ecliptic $\lambda_{Sun}$ as well as the obliquity angle $\varepsilon$ of the ecliptic over the equator. The secular variation of semi-major axis due to Earth's oblateness and solar radiation pressure without considering eclipses is zero.

In order to compare the integration of the dynamics with the semi-analytical approach with the integration with Differential Algebra techniques, it is convenient, as will be clear later, to write Eq. 4 and 5 using $\nu$ as independent variable, so that the state of the ODE system is made of the five Keplerian elements and time as $\boldsymbol{x} = (a, e, i, \Omega, \omega, t)$. The new set of equations can be simply obtained computing $\frac{d\overline{\nu}}{dt}$ due to the two body problem and the effects of $J_2$ and SRP and then

$$\frac{d\mathbf{x}}{dt} = \left\{ \begin{array}{c} \frac{d\overline{a}}{dt} / \frac{d\overline{\nu}}{dt} \\ \frac{d\overline{e}}{dt} / \frac{d\overline{\nu}}{dt} \\ \frac{d\overline{i}}{dt} / \frac{d\overline{\nu}}{dt} \\ \frac{d\overline{\Omega}}{dt} / \frac{d\overline{\nu}}{dt} \\ \frac{d\overline{\omega}}{dt} / \frac{d\overline{\nu}}{dt} \\ 1 / \frac{d\overline{\nu}}{dt} \end{array} \right\}$$

## NOTES ON DIFFERENTIAL ALGEBRA

Differential Algebra (DA) techniques, exploited here to implement a high-order orbit determination algorithm, were devised to attempt solving analytical problems through an algebraic approach.[10] Historically, the treatment of functions in numerics has been based on the treatment of numbers, and the classical numerical algorithms are based on the mere evaluation of functions at specific points. DA techniques rely on the observation that it is possible to extract more information on a function rather than its mere values. The basic idea is to bring the treatment of functions and the operations on them to computer environment in a similar manner as the treatment of real numbers. Referring to Figure 1, consider two real numbers $a$ and $b$. Their transformation into the floating point representation, $\overline{a}$ and $\overline{b}$ respectively, is performed to operate on them in a computer environment. Then, given any operation $*$ in the set of real numbers, an adjoint operation $\circledast$ is defined in the set of floating point (FP) numbers so that the diagram in Figure 1 (left) commutes. (The diagram commutes approximately in practice due to truncation errors.) Consequently, transforming the real numbers $a$ and $b$ into their FP representation and operating on them in the set of FP numbers returns the same result as carrying out the operation in the set of real numbers and then transforming the achieved result in its FP representation. In a similar way, let us suppose two $k$ differentiable functions $f$ and $g$ in $n$ variables are given. In the framework of differential algebra, the computer operates on them using their $k$-th order Taylor expansions, $F$ and $G$ respectively. Therefore, the transformation of real numbers in their FP representation is now substituted by the extraction of the $k$-th order Taylor expansions of $f$ and $g$. For each operation in the space of $k$ differentiable functions, an adjoint operation in the space of Taylor polynomials is defined so that the corresponding diagram commutes; i.e., extracting the Taylor expansions of $f$ and $g$ and operating on them in the space of Taylor polynomials (labeled as ${}_kD_n$ ) returns the same result as operating on $f$ and $g$ in the original space and then extracting the Taylor expansion of the resulting function.

The straightforward implementation of differential algebra in a computer allows computation of the Taylor coefficients of a function up to a specified order $k$, along with the function evaluation, with a fixed amount of effort. The Taylor coefficients of order $n$ for sums and products of functions, as well as scalar products with reals, can be computed from those of summands and factors; therefore, the set of equivalence classes of functions can be endowed with well-defined operations, leading to the so-called truncated power series algebra.[11,12] Similarly to the algorithms for floating point arithmetic, the algorithms for functions followed, including methods to perform composition of functions, to invert them, to solve nonlinear systems explicitly, and to treat common elementary

functions.[13,10] In addition to these algebraic operations, the DA framework is endowed with differentiation and integration operators, therefore finalizing the definition of the DA structure. The DA sketched in this section was implemented by M. Berz and K. Makino in the software COSY INFINITY.[14]

**High-order expansion of the flow**

Differential algebra allows the derivatives of any function $f$ of $n$ variables to be computed up to an arbitrary order $k$, along with the function evaluation. This has an important consequence when the numerical integration of an ODE is performed by means of an arbitrary integration scheme. Any integration scheme is based on algebraic operations, involving the evaluation of the ODE right hand side at several integration points. Therefore, carrying out all the evaluations in the DA framework allows differential algebra to compute the arbitrary order expansion of the flow of a general ODE with respect to the initial condition.

Without loss of generality, consider the scalar initial value problem

$$\begin{cases} \dot{x} = f(x,t) \\ x(t_0) = x_0 \end{cases} \tag{6}$$

and the associated phase flow $\varphi(t;x_0)$. We now want to show that, starting from the DA representation of the initial condition $x_0$, differential algebra allows us to propagate the Taylor expansion of the flow in $x_0$ forward in time, up to the final time $t_f$.

Replace the point initial condition $x_0$ by the DA representative of its identity function up to order $k$, which is a $(k+1)$-tuple of Taylor coefficients. (Note that $x_0$ is the flow evaluated at the initial time; i.e, $x_0 = \varphi(t_0;x_0)$.) As for the identity function only the first two coefficients, corresponding to the constant part and the first derivative respectively, are non zeros, we can write $[x_0]$ as $x_0 + \delta x_0$, in which $x_0$ is the reference point for the expansion. If all the operations of the numerical integration scheme are carried out in the framework of differential algebra, the phase flow $\varphi(t;x_0)$ is approximated, at each fixed time step $t_i$, as a Taylor expansion in $x_0$.

For the sake of clarity, consider the forward Euler's scheme

$$x_i = x_{i-1} + f(x_{i-1})\Delta t \tag{7}$$

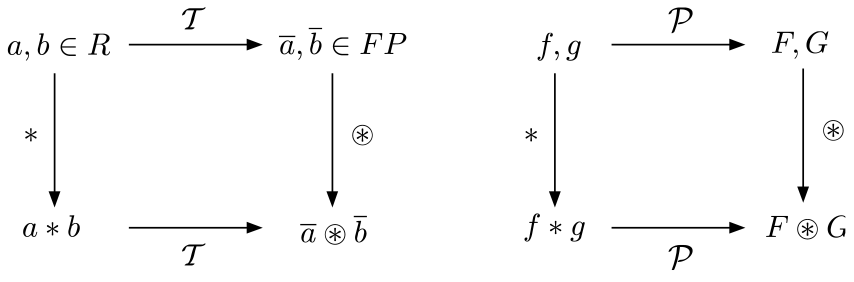


**Figure 1. Analogy between the floating point representation of real numbers in a computer environment (left) and the introduction of the algebra of Taylor polynomials in the differential algebraic framework (right).**

and substitute the initial value with the DA identity $[x_0] = x_0 + \delta x_0$. At the first time step we have

$$[x_1] = [x_0] + f([x_0]) \cdot \Delta t. \tag{8}$$

If the function $f$ is evaluated in the DA framework, the output of the first step, $[x_1]$, is the $k$-th order Taylor expansion of the flow $\varphi(t; x_0)$ in $x_0$ for $t = t_1$. Note that, as a result of the DA evaluation of $f([x_0])$, the $(k+1)$-tuple $[x_1]$ may include several non zeros coefficients corresponding to high-order terms in $\delta x_0$. The previous procedure can be inferred through the subsequent steps. The result of the final step is the $k$-th order Taylor expansion of $\varphi(t; x_0)$ in $x_0$ at the final time $t_f$. Thus, the flow of a dynamical system can be approximated, at each time step $t_i$, as a $k$-th order Taylor expansion in $x_0$ in a fixed amount of effort.

The conversion of standard integration schemes to their DA counterparts is straightforward both for explicit and implicit solvers. This is essentially based on the substitution of the operations between real numbers with those on DA numbers. In addition, whenever the integration scheme involves iterations (e.g. iterations required in implicit and predictor-corrector methods), step size control, and order selection, a measure of the accuracy of the Taylor expansion of the flow needs to be included.

The main advantage of the DA-based approach is that there is no need to write and integrate variational equations in order to obtain high-order expansions of the flow. This result is basically obtained by the substitution of operations between real numbers with those on DA numbers, and therefore the method is ODE independent. Furthermore, the efficient implementation of the differential algebra in COSY INFINITY allows us to obtain high-order expansions with limited computational time.

In particular, we point out that with this method it is possible to perform a direct DA integration of both the full dynamics as well as the averaged dynamical systems introduced in the previous section. We use a $7/8$ order Runge-Kutta integrator scheme with automatic step size control for the integration of the dynamics starting with a DA representation of the initial condition. This allows us to compute the flow expansion to arbitrary order in terms of the initial conditions at final time $t$.

For the remainder of this paper, we shall refer to the numerical DA integration simply as *DA integration*, and *full DA integration (FDI)* and *averaged DA integration (ADI)* shall refer to the DA integration of the full and averaged dynamics respectively. Furthermore, the terms *full pointwise integration (FPI)* and *averaged pointwise integration (API)* shall refer to the classical pointwise numerical integration of the full and averaged dynamics, respectively, using (potentially vectorized) floating point arithmetic.

While straightforward to implement, the DA integration method can be very time consuming if the integration is difficult and the right hand side requires small step sizes. This leads to the DA mapping method, which can mitigate this effect for certain types of repetitive systems.

## DA TRANSFER MAP METHOD

The DA mapping method for the propagation of initial state vectors in quasi-periodic dynamical systems reduces the number of integrations required in order to perform the propagation by replacing the repeated integrations by the evaluation of a Poincaré map or Poincaré-like map of the system. A polynomial expansion $\mathcal{M}$ of this Poincaré map can be computed as a high-order polynomial expansion using the DA method for the expansion of the flow described in the previous section. This polynomial map $\mathcal{M}$, also referred to as the *transfer map*, then connects the initial state vectors

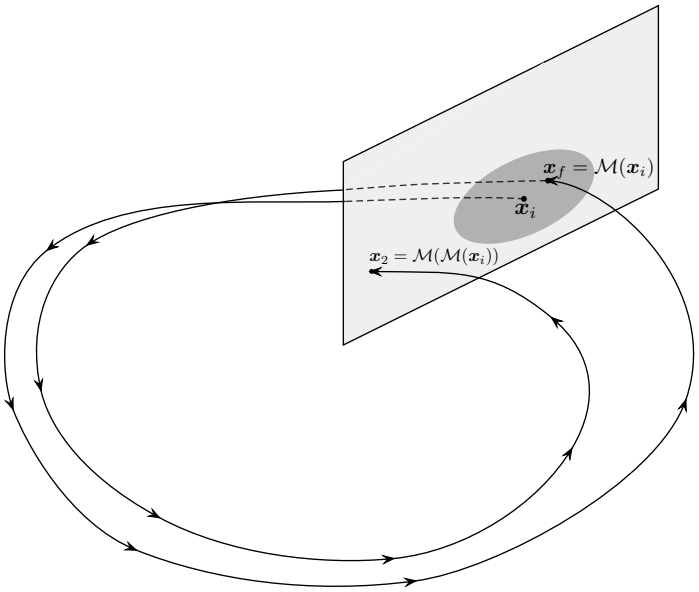


**Figure 2. Illustration of the effect of a Poincaré map in the repetitive mapping of an initial condition.**

$\boldsymbol{x}_i$ of the system to the final state $\boldsymbol{x}_f$ after one revolution in the system, i.e.

$$\mathcal{M}(\boldsymbol{x}_i) = \boldsymbol{x}_f,$$

as illustrated in Figure 2.

The computation of $\mathcal{M}$ using DA is typically much more computationally expensive than integration of one single initial condition. Once computed, however, the evaluation of such a polynomial map is usually much faster than the integration using a typical numerical integration scheme such as Runge-Kutta or Adams-Bashforth. This is because instead of computing many single steps along the orbit to reach the final state, only one simple evaluation of a polynomial is required to obtain the result for a full turn.

The advantage of the use of Poincaré maps for propagation results from the fact that once computed the same map $\mathcal{M}$ can be applied repeatedly to an initial condition to propagate it not for a single turn but for a larger number of turns without having to recompute the map. That is, given an initial condition $\boldsymbol{x}_0$, one can define the sequence $\boldsymbol{x}_n = \mathcal{M}\left(\boldsymbol{x}_{n-1}\right)$, where $\boldsymbol{x}_n$ is the state vector corresponding to the initial condition $\boldsymbol{x}_0$ after $n$ turns.

The limitation of the method is that the polynomial map $\mathcal{M}$ has a radius of convergence around the expansion point within which it represents the true map with a sufficiently high accuracy. Given such an accuracy, this defines the *region of validity* within which the map can be used to approximate the real dynamics (illustrated by the shaded area in Figure 2). Outside of this region of validity, the accuracy of the polynomial approximation is not sufficient and the map cannot be used. Thus, once one of the iterates $\boldsymbol{x}_n$ lies outside of the region of validity, the map $\mathcal{M}$ cannot be used for further iteration. Instead, a new map expansion $\mathcal{M}^*$ has to be computed that is valid in a neighborhood around the point $\boldsymbol{x}_n$. This is illustrated by the point $\boldsymbol{x}_2$ in Figure 2.

Therefore, an ideal application of the DA transfer map method is propagating around a stable periodic orbit. In this case, all points near the stable orbit stay close by, and hence one single

map can be used repeatedly to quickly propagate states. We remark in passing that this is exactly the situation in the world of particle accelerator physics, from where this DA transfer map method originates. In this field it is used to describe the motion of particles relative to a periodic reference orbit in a circular accelerator, such as the LHC at CERN.[12,15] In the case of particle accelerators, one single transfer map typically fully describes the relevant part of the dynamics of the system.

In this paper, we extend the method and apply it to state vectors in astrodynamics. In particular, we consider the motion under perturbed two-body dynamics around the Earth. The underlying dynamical problem here is not quite as well adapted to the transfer map method as is the case with particle accelerators. This is because while the unperturbed two-body motion is indeed periodic, the perturbations typically cause a long-term drift in phase space. Due to this, it is generally not possible to use a single map for all iterations, but a new map has to be computed after some number of turns.

As mentioned earlier, we chose as coordinates the Keplerian elements and time $\boldsymbol{x} = (a, e, i, \Omega, \omega, t)$ as the dependent variables, and the true anomaly $\nu$ as the independent variable. Their evolution is described by an ordinary differential equation in Gauss' form

$$\frac{d}{d\nu}\boldsymbol{x}(\nu) = \boldsymbol{X}\left(\boldsymbol{x}(\nu), \nu\right)$$

where the right hand side $\boldsymbol{X}$ includes the effect of the perturbations introduced in the section "Semi-Analytical Approach for Orbital Dynamics". The advantage of this parametrization is that the variable $\nu$ is periodic, i.e.

$$\boldsymbol{X}\left(\boldsymbol{x}(\nu), \nu\right) = \boldsymbol{X}\left(\boldsymbol{x}(\nu), \nu \mod 2\pi\right). \tag{9}$$

It is thus possible to directly compute the transfer map $\mathcal{M}$ which takes the variable $\boldsymbol{x}(0)$ to $\boldsymbol{x}(2\pi)$ by simple DA integration of the ODE. The periodicity property in Eq. 9 then allows the repeated application of $\mathcal{M}$ to compute subsequent states $\boldsymbol{x}(n \cdot 2\pi)$ as long as the previous state lies within the region of validity of the map $\mathcal{M}$.

In our algorithm, the initial expansion point around which the first polynomial map $\mathcal{M}_1$ is computed is chosen to be the initial state vector $\boldsymbol{x}_i$. The map $\mathcal{M}_1$ then represents a good approximation of the true dynamics in some neighborhood $B$ of the expansion point.

The exact size of this neighborhood depends on many factors including the particular right hand side being considered, the order of the polynomial expansion, the expansion point, as well as the accuracy requirement. While it is difficult to predict the neighborhood $B$ a priori, its size can easily be determined by manual experimentation. While in principle it is possible to construct an automated algorithm to estimate the region of validity, for this paper we implemented a simple algorithm that uses each map for a specified number of turns before automatically switching to a new map.

The order of the map expansion is variable and chosen in accordance with the problem at hand. In general, the larger the expansion order the larger is the region of validity. However, higher expansion orders also require exponentially higher computational time, so that at some point the cost of computing two low order maps becomes more favorable than one high order map. This means there is some balance between the number of maps, the expansion order and the accuracy required that depends on the problem under consideration.

The advantage of this method is that it operates on the full dynamics of the system without relying on averaging or otherwise approximating the dynamics. By controlling the re-expansion of the map

the accuracy of the method relative to the full numerical computation can be adjusted to match the needs of the application. Furthermore, this method can in principle handle any form of perturbation including non periodic perturbations. Lastly, it only requires the implementation of the perturbing force acting on the body, no manual preparation of the equations, as in the case of averaging, is required. It is thus easily adaptable to different types of perturbations.

In the application of this method to celestial mechanics in particular, there are some limitations resulting from the fundamental limitation that orbits need to be quasi-periodic. Typical perturbations, and hence the resulting dynamics, are not time independent, as the position of the celestial bodies depends on time. However time, which is one of our phase space variables, is of course monotonically increasing along each orbit. Thus any map $\mathcal{M}$ expanded around a point $(a_0, e_0, i_0, \Omega_0, \omega_0, t_0)$ will always become invalid after some number of revolutions as time invariably eventually leaves the region of validity. The size of the interval of validity around $t_0$ in time depends on the perturbation itself, the expansion order, and the initial condition. However, if the orbit under consideration is fast compared to the change of the perturbation with time, a single map expanded in time may still be valid for enough turns to make the method viable. Note that this requirement on the different speeds of the dynamics is similar to the requirement for the semi-analytical averaging. To mitigate the problem further, it is possible to increase the computation order of the time variable only, producing a polynomial expansion of the map up to a high order, e.g. 12, in time while using a lower order in for the expansion of the other phase space variables.

For the remainder of this paper, we shall refer to the propagation of a DA initial condition in the full and averaged dynamics using DA transfer maps simply as *full DA mapping (FDM)* and *averaged DA mapping (ADM)* respectively. Furthermore, the terms *full pointwise mapping (FPM)* and *averaged pointwise mapping (APM)* shall refer to the propagation of floating point initial conditions under the full and averaged dynamics respectively.

## APPLICATIONS

In this section we present two applications of the DA transfer map method.

The first example is a sun-synchronous groundtrack repeating orbit (of a satellite belonging to the COSMO-SkyMed constellation) evolving under the effect of atmospheric drag and $J_2$. This example demonstrates in detail how the DA transfer map method works and highlights some of its properties.

The second example is an heliotropic orbit of high eccentricity for a high area-to-mass spacecraft evolving under solar radiation pressure and $J_2$. In this example, we perform an exhaustive comparison between various propagation techniques for both the full and averaged dynamics when applied to the propagation of clouds of initial conditions, such as debris clouds.

### Application to Low Earth Orbits

To demonstrate the DA mapping method as described in the previous section, we now apply it to the propagation of a sun-synchronous groundtrack repeating orbit considering only the effects of $J_2$ and drag. Both of these effects do not depend on time, leading to an autonomous right hand side. This example therefore poses a good test case to demonstrate how the mapping method works without the added complication of time dependence.

The initial conditions used are

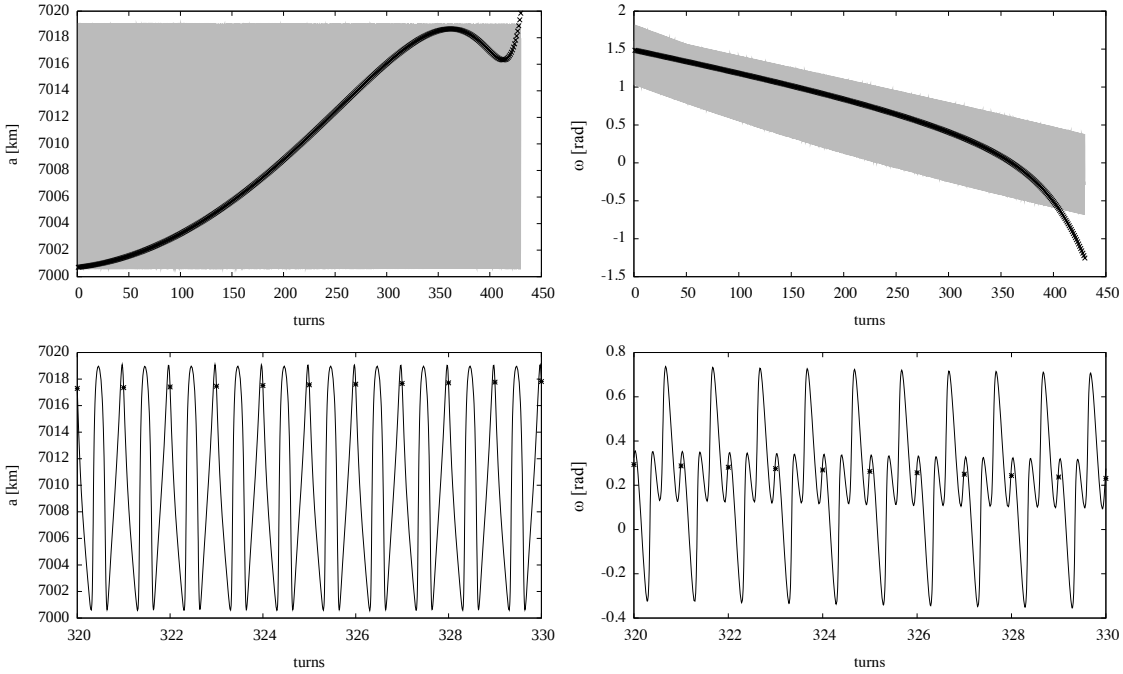


**Figure 3. The evolution of $a$ and $\omega$ propagated using pointwise integration and a single DA transfer map for $420$ turns (top) and an enlarged view of the evolution between $320$ and $330$ turns (bottom).**

$$
\begin{aligned}
a_0 &= 7000.7 \text{ km} \\
e_0 &= 0.001433 \\
i_0 &= 97.8723 \text{ deg} \\
\Omega_0 &= 204.9974 \text{ deg} \\
\omega_0 &= 85.2022 \text{ deg} \\
t_0 &= 0 \text{ sec.}
\end{aligned}
$$

First, we show the effect of a single map expanded around these initial conditions up to order $5$ in each state variable. This map $\mathcal{M}_1$ is computed and then used to propagate the initial condition repeatedly. In Figure 3 (top row), the evolution of the dependent variables $a$ and $\omega$ is shown as an representative example of the evolution of the Keplerian elements as a function of the number of turns. The solid gray line indicates the numerical reference orbit obtained by a direct integration of the ODE. Due to the fast oscillations in each turn, the orbit appears as a gray band in the graphs. The black markers indicate the results after each subsequent evaluation of the map $\mathcal{M}_1$. In Figure 3 (bottom row) an enlarged version of the plot is shown between 320 and 330 turns. These enlarged graphs show clearly that the mapped points coincide very well with the numerical orbit.

It is apparent that for a large number of turns, the numerical orbit and the points propagated by the map are in agreement. However, after about $400$ turns for $\omega$ and $420$ turns for $a$ the numerically integrated orbit is visibly different from the diverging mapped points.

This illustrates the limited region of validity of the map: at this time the orbit has left the region

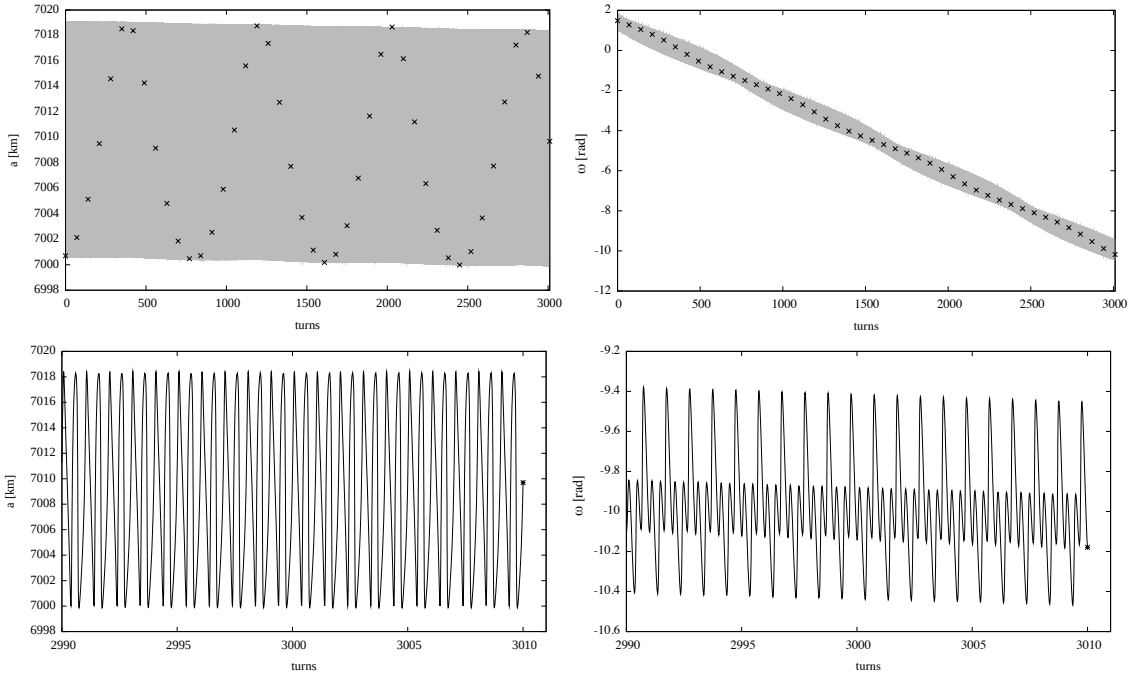


**Figure 4. The evolution of $a$ and $\omega$ propagated using pointwise integration and a sequence of $43$ DA transfer maps for $70$ turns each (top) and an enlarged view of the final $20$ turns including the final result of the mapping.**

of convergence of the map $\mathcal{M}_1$. In order to continue the propagation, a new map $\mathcal{M}_2$ has to be computed around the current propagation point. This choice of the number of turns per map provides a way to weigh accuracy of the final result vs. computational effort. The longer a single map is used, the fewer maps need to be computed, but at the same time the more truncation error is incurred. As is the case with numerical integrators, the error incurred in each map must be kept very small in order for the final error after many maps to remain small.

This is why despite the graphs shown above, we manually select the number of turns per map for the multi-map propagation to be $70$. We then continue the algorithm and recompute a new transfer map around the current point after every $70$ turns. We repeat this process for $43$ maps, propagating the initial condition for $3010$ turns or about $200$ days. Figure 4 shows the full numerical orbit of the initial condition along with a marker at the end of each of the $43$ maps, i.e. one mark every $70$ turns. As can be seen, both the numerically integrated orbit as well as the mapped results are in qualitatively good agreement.

Note that the points produced by the DA transfer map method follow a long term oscillation along the correct numerical orbit. This is due to the fact that the method uses the real full dynamics and one turn is defined as one turn of the true anomaly $\nu$. If $\omega$ changes noticeably during one turn, one revolution in $\nu$ can mean more than one revolution in physical space. In contrast to averaging methods, which consider all the orbital elements apart of $\nu$ constant during one revolution, the DA transfer map method takes this change during one revolution into account. A different choice of coordinates, such as non-singular elements would limit this oscillation, which is an artifact of circular orbits. This causes the drift in the position of the mapped points along the numerical orbit. The long term decrease of $a$ visible in the graphs is due to the effect of the atmospheric drag.

| *turns/map* | $\delta a$ [*m*] | $\delta e$ [$-$] | $\delta i$ [*rad*] | $\delta\Omega$ [*rad*] | $\delta\omega$ [*rad*] | $\delta t$ [*sec*] | $t_C$ [*sec*] |
|---|---|---|---|---|---|---|---|
| 40 | 0.28 | $4.1 \cdot 10^{-8}$ | $2.8 \cdot 10^{-9}$ | $1.2 \cdot 10^{-7}$ | $3.2 \cdot 10^{-6}$ | 0.35 | 300 |
| 50 | 1.2 | $1.7 \cdot 10^{-7}$ | $1.2 \cdot 10^{-8}$ | $4.6 \cdot 10^{-7}$ | $1.8 \cdot 10^{-5}$ | 1.4 | 240 |
| 60 | 3.8 | $4.9 \cdot 10^{-7}$ | $3.7 \cdot 10^{-8}$ | $1.3 \cdot 10^{-6}$ | $7.3 \cdot 10^{-5}$ | 4.0 | 202 |
| 70 | 8.3 | $1.1 \cdot 10^{-6}$ | $8.1 \cdot 10^{-8}$ | $2.0 \cdot 10^{-6}$ | $2.2 \cdot 10^{-4}$ | 6.2 | 175 |
| 80 | 12.7 | $1.5 \cdot 10^{-6}$ | $1.2 \cdot 10^{-7}$ | $4.3 \cdot 10^{-6}$ | $5.3 \cdot 10^{-4}$ | 13.7 | 153 |

**Table 1. Accuracy of the final condition when propagated by DA transfer maps with varying numbers of turns per map along with the computational time $t_C$ for each case.**

To further study the effect of the number of turns per map on the accuracy, we computed the error $\delta\boldsymbol{x}$ of the final state between the result of the pointwise integration and the DA transfer map. As expected, for the same setup as above, the error increases as the number of turns per map is increased. This relationship is illustrated in Table 1. As for the computational effort, we observe that the required computational time is linear in the number of maps computed, i.e. inverse proportional to the number of turns/map. We remark that also the choice of computation order affects the accuracy in the sense that a higher computation order results in a larger radius of convergence and hence a larger number of turns per map for the same accuracy requirement.

To put the computational times in Table 1 into perspective, consider that on our iMac with a 2.9 GHz Intel Core i5 processor the time to integrate only the trajectory of a single point along the reference orbit was 102 seconds. Furthermore, one important feature of the DA transfer map method is that the computational time practically does not depend on what is being propagated. The computational effort of evaluating the maps with a single point, a vector of a large number of points, or even a DA expansion in the initial conditions is negligible compared to the time taken to compute the transfer maps. Thus the cost of propagating one single point or a cloud of 10.000 points is the same with the DA transfer map method. For the pointwise integration, however, it is clear that the integration of additional points comes at a higher additional cost, even if vectorization features of modern CPUs are used.

To demonstrate this important feature of the DA transfer map method, Table 2 shows the computational time to propagate various objects in the same setup as before once by pointwise integration and once by DA transfer maps with 70 turns per map. The initial conditions are either the given number of randomly chosen points within the uncertainties as a vector of points, or a DA expansion of the initial conditions covering the uncertainty box. We use the following bounds on initial condition uncertainties:

$$\begin{aligned} a_0 &= 7000.7 \text{ km} \pm 0.1 \text{ km} \\ e_0 &= 0.001433 \pm 5 \cdot 10^{-5} \\ i_0 &= 97.8723 \text{ deg} \pm 10^{-4} \cdot \frac{180}{\pi} \text{ deg} \\ \Omega_0 &= 204.9974 \text{ deg} \pm 10^{-4} \cdot \frac{180}{\pi} \text{ deg} \\ \omega_0 &= 85.2022 \text{ deg} \pm 10^{-3} \cdot \frac{180}{\pi} \text{ deg} \\ t_0 &= 0 \text{ sec} \pm 60 \text{ sec}. \end{aligned}$$

As is clearly visible, the computational time for the DA transfer map method remains constant, while the numerical integration requires significantly more time even for a relatively small number

| *Initial condition* | *Integration* $[s]$ | *Transfer Maps* $[s]$ |
|---|---|---|
| 10 points | 160 | 169 |
| 100 points | 404 | 171 |
| 1.000 points | 2533 | 167 |
| DA | 12445 | 169 |

**Table 2. Computation time in seconds to propagate the given number of points or a DA expansion by integration and DA transfer maps.**

of points. From the last row of Table 2 it is apparent that the time taken to compute the expansion of the flow is two orders of magnitude larger for the DA integration as described in subsection "High-order expansion of the flow" than for the DA mapping method.

### Performance Comparison on Heliotropic Orbits

To compare the performance of the various methods to propagate sets of initial conditions, we select another test case. The two-body dynamics of a spacecraft with high area-to-mass ratio orbiting the Earth is strongly perturbed by the term of the gravitational field due to the Earth's oblateness and by the effect of solar radiation pressure. The orbit evolution shows an interesting behaviors in the phase space of eccentricity and $\phi$, where

$$\phi = \Omega + \omega - (\lambda_{Sun} - \pi)$$

describes the orientation of the orbit perigee with respect to the Sun. As was analyzed in a previous publication, if the obliquity angle is assumed to be zero, the system allows some equilibrium solutions which corresponds to frozen orbits with resect to the Sun.[2] The equilibrium solution $\phi = 0$ , existing at semi-major axis below approximately $15000$ km corresponds to a family of heliotropic orbits that maintain their perigee in the direction of the Sun, while $\phi = \pi$, existing for semi-major axis above $13000$ km approximately, corresponds to families of anti-heliotropic orbits, with the apogee frozen in the Sun-direction. Initial conditions around the equilibrium orbit will librate in the phase space of $e - \phi$ around the equilibrium. The eccentricity value of the equilibrium solution depends on the semi-major axis and the value of the area-to-mass ratio $A/m$ of the spacecraft, which can be used as control parameter to design frozen orbits with respect to the Sun. A detailed description of the possible solutions is given in a previous publication.[2]

In this article, we apply the methods to the propagation of orbits around the following reference orbit using a two-body model perturbed by the effect of solar radiation pressure and the effect of the $J_2$ oblateness of the earth. The reference orbit is given by the parameters

$$\begin{aligned} a_0 &= 12000 \text{ km} \\ e_0 &= 0.15 \\ i_0 &= 0 \text{ deg} \\ \Omega_0 &= 0 \text{ deg} \\ \omega_0 &= 180 \text{ deg} \\ t_0 &= 0 \text{ sec} \end{aligned} \tag{10}$$

and selecting $A/m = 15$ m$^2$/kg and $c_R = 1$. This condition corresponds to a solution which librates around the equilibrium solution $\phi = 0$ , that is a family of heliotropic orbits. Figure 5

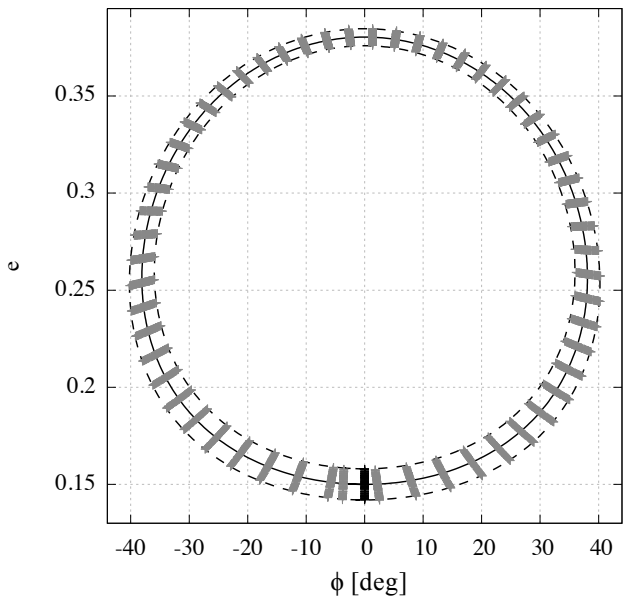


**Figure 5. Phase space diagram of $\phi$ vs. $e$ indicating the position of the propagated clouds at various times during the integration.**

represents the evolution of a cloud of points around the initial condition in Eq. 10, considering a displacement of the initial eccentricity of $e_0 \pm 8 \cdot 10^{-3}$. Each of the point in the cloud correspond to one orbit and following positions of the cloud in the phase space describe the orbit evolution with respect to the direction of the Sun. Such behavior is typical of a cloud of dust particles with high area-to-mass ratio ejected from Phobos and Deimos on orbits around Mars or high area-to-mass spacecraft around the Earth.[1,2] Similarly, this model can be used to describe the evolution of high area-to-mass ratio space debris fragments at high altitude. The representation of the evolution of the cloud allows studying the fragments evolution as a whole.

*Comparison of Propagation Methods* Next, we systematically compare all combinations of propagation methods and numerical techniques described before. We recall that in our notation introduced in previous sections each method tested is a combination of three components: the *propagator*, the *dynamics* and the *data type* being propagated.

The propagator used is either a $7/8$ order Runge-Kutta integrator with automatic step size control or the DA transfer map method described in the previous section. The dynamics are either the full dynamical system of Gauss' equations with the perturbations of solar radiation pressure, $J_2$ and atmospheric drag, or the averaged equations of the same system as introduced previously. Lastly, the data type refers to the arithmetic data type that is used to evaluate the arithmetic operations and can be either points, referring to a list of points which are propagated in parallel in a particularly efficient manner on modern CPUs, or the DA datatype introduced in section "Notes on Differential Algebra", which results in a polynomial expansion of the flow which is then evaluated with the desired initial conditions to obtain the final points.

Table 3 lists the names we introduced in the previous sections for each of the possible combinations of these three properties. For the remainder of this paper, we shall continue to use these names to identify each method.

| *Method* | *Abbreviation* | *Propagator* | *Dynamics* | *Data Type* |
|---|---|---|---|---|
| full DA integration | FDI | Integration | Full | DA |
| averaged DA integration | ADI | Integration | Averaged | DA |
| full pointwise integration | FPI | Integration | Full | Points |
| averaged pointwise integration | API | Integration | Averaged | Points |
| full DA mapping | FDM | Transfer Map | Full | DA |
| averaged DA mapping | ADM | Transfer Map | Averaged | DA |
| full pointwise mapping | FPM | Transfer Map | Full | Points |
| averaged DA mapping | ADM | Transfer Map | Averaged | Points |

**Table 3. Propagation method names and their meaning.**

To test the propagation of clouds of varying size with each propagation method, a random sample of initial conditions is selected with various values for eccentricity $e$ in the interval $e_0 \pm 8 \cdot 10^{-3}$ while all other values are kept constant at the reference values given above. The number of points investigated in this paper are $10$, $100$, $1.000$, and $10.000$. The propagation time is $5040$ turns or about $762$ days.

For the DA integrations, computations are performed up to order $4$ in $e$, and in the case of DA transfer maps order $4$ is used for the first five variables $a, e, i, \Omega, \omega$ while time $t$ is expanded up to order $12$ to account for the time dependence of the perturbation due to the motion of the Sun. By increasing the interval of validity of each map in the time variable, this allows a single map to be used for longer time and thus more turns before having to recalculate a new map. The number of turns per map for the DA transfer map method is chosen to be $90$.

The resulting computational time of propagating these sets on a MacBook Air with 1.8 GHz Intel Core i5 processor is reported in Table 4 and visualized in Figure 6. As is to be expected, the propagation methods using the averaged dynamical equations far outperform the methods using the full dynamics independently of the propagator used. This is due to the fact that the averaging removes the short term oscillations from the right hand side, thus rendering the resulting ODE less stiff and allowing much larger integration steps in the underlying Runge-Kutta integration scheme. Another noteworthy result is that all DA based methods show quasi constant computational cost in terms of the number of points propagated. This is also the expected result as the cost of evaluating the final polynomial expansion of the flow once even for a large number of point is negligible compared to the computational cost of computing the polynomial in the first place.

For the pointwise integration methods, the computational time grows almost linearly with the number of points. For low numbers of points, on the order of $100$, the pointwise integration is faster than the DA integration methods. As soon as the number of initial conditions grows larger, however,

| *Number of Points* | *FPI* | *FDI* | *API* | *ADI* | *FPM* | *FDM* | *APM* | *ADM* |
|---|---|---|---|---|---|---|---|---|
| 10 | 172 | 805 | 0.4 | 2.8 | 173 | 177 | 25 | 25 |
| 100 | 354 | 748 | 1.1 | 2.8 | 178 | 180 | 25 | 25 |
| 1.000 | 2128 | 748 | 8.4 | 2.8 | 174 | 172 | 26 | 26 |
| 10.000 | 21531 | 717 | 85 | 2.9 | 168 | 167 | 27 | 26 |

**Table 4. Computation time in seconds to propagate the given number of initial points varying in $e$ using each propagation method.**

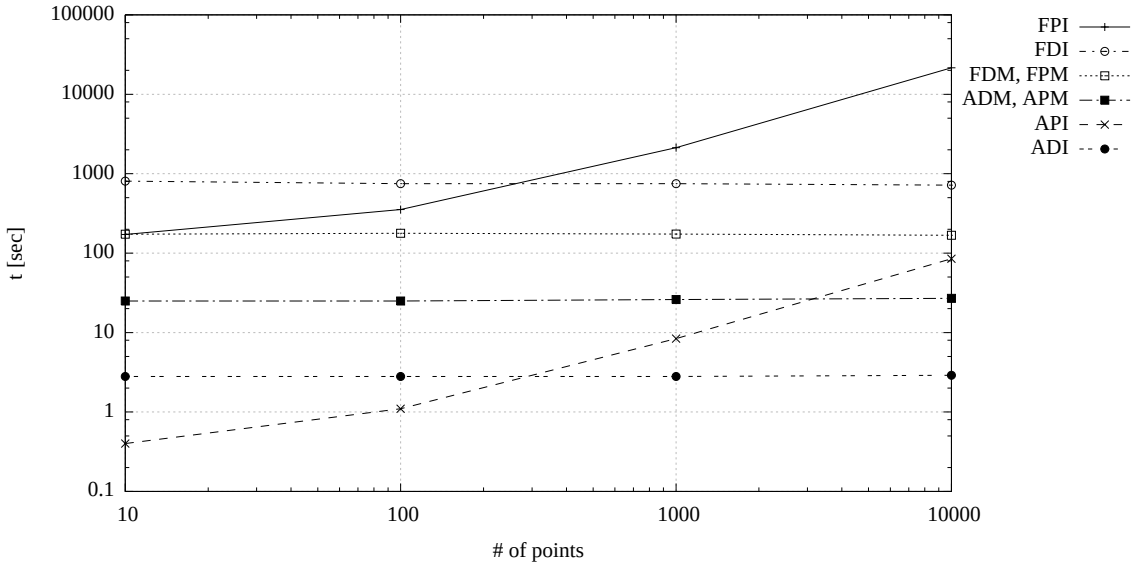


**Figure 6. Computational time as a function of the number of initial states varying in $e$ propagated using each method.**

the DA integration methods as well as the DA transfer map methods become more favorable. We remark that in practice the number of points propagated is typically much larger than his threshold. Once uncertainties in all $6$ dimensions of phase space are considered, the number of vertices of this $6$ dimensional cube alone is already $64$, and that would only propagate the extremal points of the uncertainty set without any points in its interior.

*High Order Flow Expansion of Averaged Equations* In the above comparison, we only consider uncertainties in one single variable, the eccentricity $e$. As has been shown, already the computation of a high order flow expansion in just this one variable over a relatively small uncertainty is a difficult task when using the full dynamics. However, in real world applications uncertainty is typically present in all phase space variables.

From the previous full comparison, we identify the following promising propagation methods capable of computing a high order flow expansion in all phase space variables within a reasonable amount of time:

1. Integration of the averaged dynamics in DA arithmetic (ADI)

2. Transfer maps of the averaged dynamics in DA arithmetic (ADM)

3. Transfer maps of the full dynamics in DA arithmetic (FDM)

Each one of these methods is tested by propagating the following box of initial uncertainties as a

| *Method* | ADI | ADM | FDM |
|---|---|---|---|
| *Time* $[s]$ | 25 | 27 | 201 |

**Table 5. Computation time to compute a full high order flow expansion with each method.**

DA expansion in the same setting as before:

$$\begin{aligned} a_0 &= 12000 \text{ km} \pm 0.1 \text{ km} \\ e_0 &= 0.15 \pm 0.8 \cdot 10^{-3} \\ i_0 &= 0 \text{ deg} \pm 10^{-4} \cdot \frac{180}{\pi} \text{ deg} \\ \Omega_0 &= 0 \text{ deg} \pm 10^{-4} \cdot \frac{180}{\pi} \text{ deg} \\ \omega_0 &= 180 \text{ deg} \pm 10^{-3} \cdot \frac{180}{\pi} \text{ deg} \\ t_0 &= 0 \text{ sec} \pm 60 \text{ sec}. \end{aligned}$$

The times taken for each of these propagations are reported in Table 5. As expected, both methods based on the averaged dynamics (ADI, ADM) are significantly faster than the DA transfer maps of the full dynamics (FDM). However, for the computation of the full map expansion both DA transfer maps and integration of the averaged dynamics (ADI and ADM) are comparable in computational time. This result once more illustrates the fact that DA transfer maps have constant computational cost independently of the propagated initial conditions, while the computation of the flow expansion in all six phase space variables results in a significant change in the computational time for the integration methods compared to the flow expansion in one single phase space variable.

## CONCLUSIONS

In this paper, we introduced propagation using the DA transfer map method which allows the fast propagation of initial conditions in dynamics exhibiting repetitive motion. The accuracy and computational speed of the method have been demonstrated with various examples and compared to other long-term propagation techniques based on averaging and the integration of the full dynamics. Key features, such as the independence of the computational cost with respect to the number or type of initial conditions, have been analyzed.

When compared to numerical integration of the full dynamics, the map method is orders of magnitude faster, particularly for large sets of initial conditions or for the high order expansion of the flow using DA.

Comparison with averaged dynamics shows that if averaged equations provide results of sufficient accuracy for the problem at hand then the DA integration or the DA transfer map method applied to the averaged equations (ADI, ADM) are the best options in terms of computational time for the propagation of clouds. On the other hand, if highly accurate result are required, the DA transfer maps applied to the full dynamics (FDM) allow the propagation of osculating parameters with moderate additional cost in computational time.

Future research on the combination of differential algebra techniques, averaged equations, and DA transfer maps is expected to yield fast and accurate methods to propagate large clouds of initial conditions very efficiently.

## ACKNOWLEDGMENTS

C. Colombo acknowledges the support received by the Marie Curie grant 302270 (SpaceDebECM - Space Debris Evolution, Collision risk, and Mitigation). A. Wittig gratefully acknowledges the support received by the Marie Curie fellowship PITN-GA 2011-289240 (AstroNet-II).

## REFERENCES

[1] A. V. Krivov, L. L. Sokolov, and V. V. Dikarev, "Dynamics of Mars-Orbiting Dust: Effects of Light Pressure and Planetary Oblateness," *Celestial Mechanics and Dynamical Astronomy*, Vol. 63, No. 3, 1995, pp. 313–339, 10.1007/bf00692293. (document)

[2] C. Colombo, C. Lücking, and C. McInnes, "Orbital Dynamics of High Area-to-Mass Ratio Spacecraft with $J_2$ and Solar Radiation Pressure for Novel Earth Observation and Communication Services," *Acta Astronautica*, Vol. 81, No. 1, 2012, pp. 137–150, 10.1016/j.actaastro.2012.07.009. (document)

[3] S. Valk, N. Delsate, A. Lemaître, and T. Carletti, "Global dynamics of high area-to-mass ratios GEO space debris by means of the MEGNO indicator," *Advances in Space Research*, Vol. 43, No. 10, 2009, pp. 1509–1526, 10.1016/j.asr.2009.02.014. (document)

[4] M. Berz, *Differential Algebraic Techniques, Entry in Handbook of Accelerator Physics and Engineering*. New York: World Scientific, 1999. (document)

[5] M. Berz, "Differential Algebraic Techniques," *Entry in the Handbook of Accelerator Physics and Engineering*, 1998. (document)

[6] R. Armellin, P. D. Lizia, F. B. Zazzera, and M. Berz, "Asteroid Close Encounter Characterization using Differential Algebra: the Case of Aphophis," *Celestial Mechanics and Dynamical Astronomy*, Vol. 107, No. 4, 2010. (document)

[7] C. Colombo, E. M. Alessi, and M. Landgraf, "End-of life disposal of spacecraft in Highly Elliptical Orbits by means of luni-solar perturbations and Moon resonances," Sixth European Conference on Space Debris, Darmstadt, Germany, ESA/ESOC, 22-25 April 2013. (document)

[8] R. Battin, *An Introduction to the Mathematics and Methods of Astrodynamics*. Reston, VA: AIAA Education Series, 1999. (document)

[9] D. A. Vallado, *Fundamentals of Astrodynamics and Applications*. New York: Space Technology Library, third edition ed., 2007. (document)

[10] M. Berz, *Modern Map Methods in Particle Beam Physics*. Academic Press, 1999. (document)

[11] M. Berz, *The new method of TPSA algebra for the description of beam dynamics to high orders*. Los Alamos National Laboratory, 1986. Technical Report AT-6:ATN-86-16. (document)

[12] M. Berz, "The method of power series tracking for the mathematical description of beam dynamics," *Nuclear Instruments and Methods A258*, 1987. (document)

[13] M. Berz, *Differential Algebraic Techniques, Entry in Handbook of Accelerator Physics and Engineering*. New York: World Scientific, 1999. (document)

[14] M. Berz and K. Makino, *COSY INFINITY version 9 reference manual*. Michigan State University, East Lansing, MI 48824, 2006. MSU Report MSUHEP060803. (document)

[15] M. Berz, K. Makino, and K. Shamseddine, *Modern map methods in particle beam physics*, Vol. 108. Academic Press, 1999. (document)